

Performance Enhancement of Ag-Au Bimetallic Surface Plasmon Resonance Biosensor using InP

Hasan Khaled Rouf* and Tauhidul Haque

Abstract—Performance improvement of couple silver (Ag)-gold (Au) based bimetallic surface plasmon resonance (SPR) sensor using a thin indium phosphide (InP) layer and an air gap layer is presented. Through detailed investigations quantitative insight into the dependence of different performance parameters including sensitivity factor (SF), sensor merit (SM), full width at half maximum (FWHM) and combined sensitivity factor (CSF) on stack structure, thickness and material parameters has been observed. Integration of thin InP layer on the metallic layer and inclusion of the air gap between glass prism and adsorption layer enhance both the sensitivity ($70.90^\circ/\text{RIU}$) and the CSF (372.8 RIU^{-1}). Without InP layer the sensitivity is $65.66^\circ/\text{RIU}$, and CSF is 178.5 RIU^{-1} whereas without the air gap the sensitivity is $66.29^\circ/\text{RIU}$, and the CSF is 285.0 RIU^{-1} . Compared to similar bimetallic SPR sensors that have been reported in recent literatures, sensitivity and overall figure of merit of the proposed sensor are far better. The presented biosensor's capability to detect the variation of 1/1000 of RIU of the sensing medium (corresponding to subtle concentration change of the analyte) has been demonstrated.

1. INTRODUCTION

Surface plasmon resonance (SPR) technique has been used in optical sensors for chemical and biological detection for many years [1, 2], and recently it also finds applications in terahertz (THz) plasmonic devices for photodetection [3, 4]. Although SPR sensors have made significant progress, they are still unable to achieve the direct detection of small molecular interactions or low molecular concentrations on the surface of the biosensors. Consequently, various proposals have been developed to enhance the sensitivity or resolution of SPR sensors by using different SPR modes or detection methods [5]. Recently, two-dimensional (2D) layered materials, such as graphene, transition metal dichalcogenides (TMDCs), and black phosphorus (BP), have come into the picture for devising flexible photodetectors from visible to THz range [6]. These materials have exceptional electrical and optical properties, chemical stability and biocompatibility, and depending on their specific band structures they can demonstrate peculiar functionalities which can be exploited for highly efficient light detection [3, 7–9]. Graphene and graphene oxide provide good support for biomolecule adsorption due to their large surface area and rich pi-conjugation structure making them suitable dielectric top layers for SPR sensing. However, there are limitations of graphene-on-metal SPR substrates for real-time sensing, such as the lack of specificity of the interfaces and most biomolecules adsorbed on graphene; these make selective sensing rather difficult [10]. Thus, with an energy gap in-between graphene and TMDCs black phosphorus recently emerged as a fascinating and versatile material for photodetection [3, 6].

Thickness of the metallic layer, material properties, variations of the stack structure and various structural parameters affect the response and performance of the SPR sensors. Therefore, metallic layer optimization is required to improve the sensor performance [11]. Due to the presence of well-resolved

Received 25 September 2018, Accepted 5 November 2018, Scheduled 20 November 2018

* Corresponding author: Hasan Khaled Rouf (hasan.rouf@cu.ac.bd).

The authors are with the Department of Electrical & Electronic Engineering, University of Chittagong, Chittagong 4331, Bangladesh.

SPR, silver (Ag) and gold (Au) are the most commonly used metals for sensing applications [12–14]. Silver based sensors have higher spectral sensitivity while gold based sensors have higher angular sensitivity [15]. On the other hand, silver has poor chemical resistance when it is in contact with the atmosphere or some chemicals. As a result, use of gold is more prevalent because of its high chemical resistance and stable performance. To take the advantage of both metals, i.e., higher sensitivity of silver and stability and chemical resistance of gold, in this work we consider a bimetallic configuration which has been recently studied by some researchers [16–19]. In the bimetallic SPR sensor designs of [16, 17], no proper adherence material was used to fix the silver and gold layer to the glass prism despite the fact that both silver and gold have poor adherence with glass. To enhance the adhesion between metal and glass [18] incorporates a thin chromium (Cr) film on the glass substrate. Reference [19] used double pairs of dielectric-metal (Teflon-silver) multilayers between a prism and target molecule which leads to enhanced depth-to-width ratio of the reflectance curve. The relatively thick dielectric layer used in this work leads to increased SPR evanescent wave penetration depth, but the sensitivity is significantly reduced because the sensing surface is located at a considerable distance from the SPs which exist at the metal-dielectric interface [20].

This paper presents the design of a new couple Ag-Au metal film based SPR sensor with improved performance parameters. In the proposed design, with couple Ag-Au metal films, a thin layer of indium phosphide (InP) and an air gap are used. To enhance the adherence of metal layer on prism glass titanium (Ti) is used. By studying spectral and angular properties of the illuminating beams we observed the operating wavelengths and resonance angles of the proposed sensor. Characteristic transfer matrix (CTM) approach was used for the studies of the reflectance curves, and through detailed investigation of these curves we studied different performance parameters including sensitivity factor (SF), sensor merit (SM), full width at half maximum (FWHM) values and combined sensitivity factor (CSF). Spectral effects of incidence angle and metal film thickness on reflectance were studied and optimized thickness of each layer were obtained. We established the best optical properties of the metal to obtain the best performance. Compared with only-Au-layer configuration or only-Ag-layer configuration, coupled Ag-Au layer configuration provides the lowest and sharpest dip in the reflectivity curve and the best overall performance. Integration of the thin InP layer enhances the sensitivity from $65.66^\circ/\text{RIU}$ to $70.90^\circ/\text{RIU}$ and the combined sensitivity factor (an overall figure of merit of the sensor) from 178.5 RIU^{-1} to 372.8 RIU^{-1} . Performance of the proposed bimetallic sensor is far better than that of the bimetallic sensors reported in recent literature. For example, SF and CSF of the bimetallic SPR sensor of [16] are $49.17^\circ/\text{RIU}$ and 108.0 RIU^{-1} , respectively, while for the SPR sensor presented here these parameters are $70.90^\circ/\text{RIU}$ and 372.8 RIU^{-1} , respectively. Proposed SPR sensor's ability to detect very subtle variations in concentration of liquids at the ng/mL level is demonstrated by detecting the variation of $1/1000$ of RIU of the sensing medium (i.e., target material for sensing application).

2. THEORETICAL MODEL

2.1. Theory

Surface plasmons (SPs) or surface plasmon waves (SPWs) are the free-charge oscillations occurring upon incidence of light at the interface of a dielectric and a metal. Surface plasmon resonance occurs when the momentum of the SPs matches that of the incident wave. This wave-matching condition is disrupted by even very tiny changes in the interface conditions. Thus when the condition of light excitation remains unchanged, changes in the refractive index of the medium adjacent to the metal can be precisely determined by optically interrogating the SPR. To excite SP, photon momentum of the incident light beam is to be enhanced to the level of SP momentum which can be achieved by using attenuated total reflection (ATR) by prism couplers or other techniques. For surface plasmon excitation in conventional Kretschmann configuration which is based on the ATR method, a coupling prism is interfaced with a thin metal film. The evanescent wave created by the attenuated total reflection of light incident on the prism-metal interface couples with the SP if the phase matching condition is fulfilled. SPR requires the wave vector of the incident light in the plane of the surface (k_x) to match the wave vector of the SP wave in metallic films (k_{sp}):

$$k_x = n_p (2\pi/\lambda) \sin \theta \quad (1)$$

$$k_{sp} = \frac{2\pi}{\lambda} \sqrt{\frac{\epsilon_m \epsilon_d}{\epsilon_m + \epsilon_d}} \quad (2)$$

Here ϵ_d and ϵ_m represent complex dielectric constant of dielectric material and metal, respectively; n_p is the refractive index of the prism; and λ and θ are wavelength and angle of incident light, respectively. The matching relationships for SPR are $k_x = k_{sp}$ and $\theta_{res} = \sin^{-1} \sqrt{\frac{\epsilon_m \epsilon_d}{\epsilon_p(\epsilon_m + \epsilon_d)}}$ where θ_{res} is the resonant angle. k_x can be adjusted by controlling the angle of incidence in order to match the propagation constant of the plasmon waves.

The interaction of light wave with SPW can alter light's characteristics such as amplitude, phase, polarization and spectral distribution. Changes in these characteristics can be correlated with changes in the propagation constant of the SPW. Therefore, changes in the refractive index at the sensor surface and consequently the propagation constant of the SPW can be determined by measuring changes in one of these characteristics. Based on the measured characteristic, SPR sensors can be classified as angle, wavelength, intensity, phase or polarization modulation-based sensors. In the SPR biosensors, biomolecular recognition elements on the surface of metal recognize and capture analyte present in a liquid sample and produce a local increase in the refractive index at the metal surface. Increase of refractive index gives rise to an increase in the propagation constant of SPW propagating along the metal surface which can be accurately measured by optical means.

2.2. Proposed SPR Sensor Structure

The schematic diagram of the proposed SPR sensor is shown in Fig. 1 which consists of glass prism, air gap layer, titanium (Ti) layer, bimetallic layer consisting of silver (Ag) and gold (Au) films, indium phosphide (InP) layer and sensing layer which we considered to be water. Refractive indices of the prism glass, air gap and Ti are 1.723, 1.0 and $2.9838 + i4.0042$, respectively. The Ti layer is used to enhance the adherence of silver layer on glass prism. Bimetallic layers consisting of Ag and Au films are then used which have the refractive indices of $0.1468 + i4.8604$ and $0.1676 + i4.5332$, respectively. This bimetallic structure gives the advantages of both metals, that is, stability and chemical resistance of gold and higher sensitivity of silver. Thereafter, a thin InP layer having refractive index of $3.4719 + i0.23111$ [21] is used. Addition of this thin layer on top of the metal layer enables SP to spread along it and causes a larger fraction of the evanescent field to be in the analyte region. Since this layer has a large refractive index it can support guided waves for smaller thicknesses. Since the wave is partially guided and the interaction volume is larger, the sensitivity is increased [5, 22]. Finally, a sensing medium is used as the cover layer for which we considered water with refractive index 1.33.

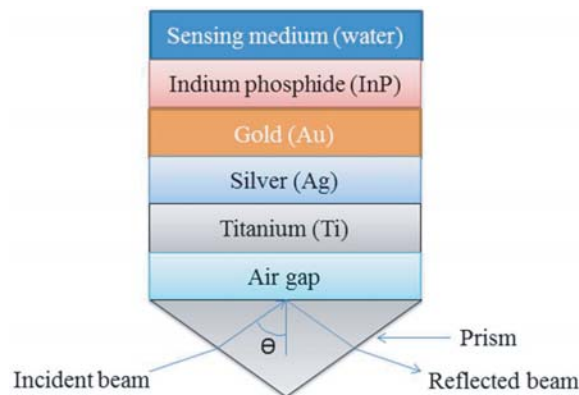


Figure 1. Schematic diagram of the proposed SPR sensor.

2.3. Characteristic Transfer Matrix (CTM) Method

We used characteristic transfer matrix method to investigate the optical characteristics of the proposed sensor. This method can be used to study reflectance and transmittance of thin films if the film thickness

is comparable to the wavelength of incident light. If there are N layers in the SPR sensor stack apart from the prism, tangential components of electric and magnetic fields at the first (E_a and B_a) and last (E_N and B_N) boundaries can be expressed as:

$$\begin{bmatrix} E_a \\ B_a \end{bmatrix} = \begin{bmatrix} N \\ \prod_{i=1} \mathbf{M}_i \end{bmatrix} \begin{bmatrix} E_N \\ B_N \end{bmatrix} = \begin{bmatrix} m_{11} & m_{12} \\ m_{21} & m_{22} \end{bmatrix} \begin{bmatrix} E_N \\ B_N \end{bmatrix} \quad (3)$$

Here \mathbf{M}_i is the individual transfer matrix of the i -th layer ($i = 1$ to N) stacked sequentially between the prism and the sensing layer and is given by

$$\mathbf{M}_i = \begin{bmatrix} \cos \delta_i & \frac{i \sin \delta_i}{\gamma_i} \\ i\gamma_i \sin \delta_i & \cos \delta_i \end{bmatrix} \quad (4)$$

Here, the optical phase addition introduced by a single traversal of the field across the layer, i.e., δ_i , is given by

$$\delta_i = \left(\frac{2\pi}{\lambda} \right) n_i d_i \cos \theta_i \quad (5)$$

where λ is the wavelength in vacuum, n_i the refractive index of the i -th layer, d_i the thickness of the i -th layer, and θ_i the incidence angle to the i -th layer. ϵ_0 and μ_0 are the permittivity and permeability in vacuum, respectively. The parameter for the individual layer γ_i for p -polarization is

$$\gamma_i = \frac{n_i \sqrt{\epsilon_0 \mu_0}}{\cos \theta_i} \quad (6)$$

The power of the CTM method can best be appreciated when dealing with multiple layers of thin films as in our case here. In Eq. (3) we related the electric and magnetic fields inside the i -th layer at both interfaces to the interference matrix \mathbf{M}_i for that layer. Since the transverse components of the electrical and magnetic fields are continuous at each interface that is free of net charge and current, the total interference matrix of the whole multilayer structure was obtained using $\mathbf{M} = \prod_{i=1}^N \mathbf{M}_i$. Then the reflection and transmission coefficients, r and t , through the films can be obtained using these matrices as follows:

$$r = \frac{\gamma_N m_{11} + \gamma_0 \gamma_N m_{12} - m_{21} - \gamma_0 m_{22}}{\gamma_N m_{11} + \gamma_0 \gamma_N m_{12} + m_{21} + \gamma_0 m_{22}} \quad (7)$$

$$t = \frac{2\gamma_0 \left(\frac{n_N}{n_0} \right)}{\gamma_N m_{11} + \gamma_0 \gamma_N m_{12} + m_{21} + \gamma_0 m_{22}} \quad (8)$$

From Eq. (7) reflectance from the multilayer stack can be calculated ($R = |r|^2$) to obtain pattern of redistribution of incident light energy into SPR waves, and thus reflected field power as a function of incident angle can be obtained. Similarly, transmission through the multilayer stack ($T = |t|^2$) can be calculated from Eq. (8).

3. RESULT AND DISCUSSION

Numerical simulation using finite difference time domain (FDTD) method was performed to study the reflectance curves and analyze the proposed SPR sensor thoroughly. Different performance parameters of the SPR sensors were used, namely, sensitivity factor (SF), sensor merit (SM) and combined sensitivity factor (CSF). Sensitivity factor is the change in resonance angle ($\delta\theta_{res}$) of the SPR sensor per unit change in the refractive index of the sensing region (δn_s) at sensor surface:

$$\text{SF} = \frac{\delta\theta_{res}}{\delta n_s} \text{ (deg/RIU)} \quad (9)$$

Due to the broadening of reflectance dip, the resolution of the sensor becomes worse, and thus the accuracy depends on the width and shape of resonance damping in the neighborhood of the minimum. This is measured by sensor merit (SM) [23]:

$$SM = \frac{1 - R_r}{FWHM} \tag{10}$$

where R_r = reflectance at resonance. For a fair comparison, a figure of merit called combined sensitivity factor (CSF) is used. CSF is the product of sensitivity and resolution of the sensor and is inversely proportional to the limit of detection of the sensor [23]:

$$CSF = SF * SM \tag{11}$$

Associated with a particular SPR sensor configuration and at a wavelength there is only one thickness that allows an optimized transfer of energy from the illuminating beam to the plasmon wave [12, 24]. Therefore, for the proposed SPR sensor at first we need to find the optimum wavelength of the illuminating beam. Fig. 2 shows the reflectance curve as a function of incidence angle at different operating wavelengths: 745 nm, 750 nm, 755 nm, 760 nm, 765 nm and 770 nm. Among these curves, the minimum of the dip in the reflectivity is 0.00339201 which is obtained when the operating wavelength is 750 nm, and the incidence angle is 45.34°. This is a resonance angle (θ_{res}) at which the minimum dip with narrow width of reflectivity curve is observed. At other wavelengths the dip goes up, and at 770 nm it is 0.040314 which is the highest among the minima. Dissipation in metal caused by absorption affects the width of the reflectance dip, and the imaginary part of metal refractive index mainly determines this. Table 1 shows real and imaginary parts of refractive indices of Ag, Au and Ti at 750 nm and 770 nm wavelengths. At larger wavelengths the imaginary parts become larger increasing the dissipation and consequently widening the dip. Full width at half maximum (FWHM) quantitatively describes the width and sharpness of the reflectance curve. Higher sensitivity in SPR sensors can be attained with sharper shapes which suggest faster recovery. For the proposed SPR sensor upon comparison of FWHM at different operating wavelengths, the best (i.e., least) value (0.189534°) was found at 750 nm. Since the FWHM of a high performance SPR sensor should be as low as possible, performance of the proposed sensor is best at 750 nm.

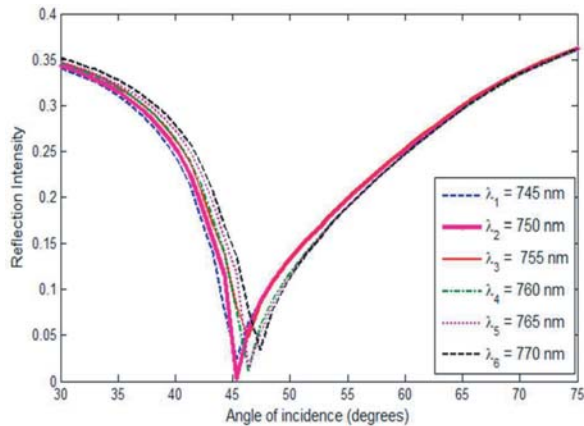


Figure 2. Reflectance curves as a function of incidence angle at different operating wavelengths (λ).

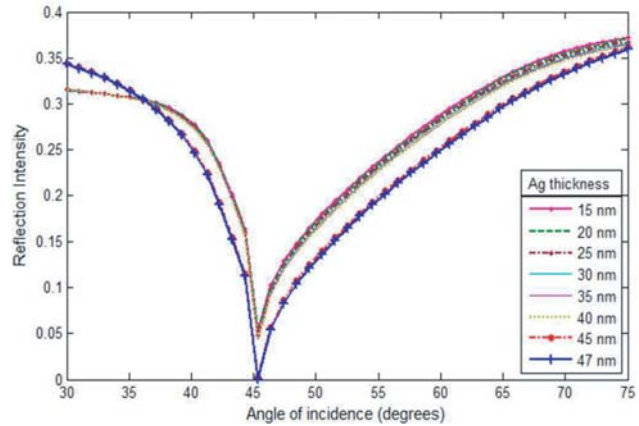


Figure 3. Variations of reflectance with different Ag layer thicknesses and constant Au layer thickness of 2 nm.

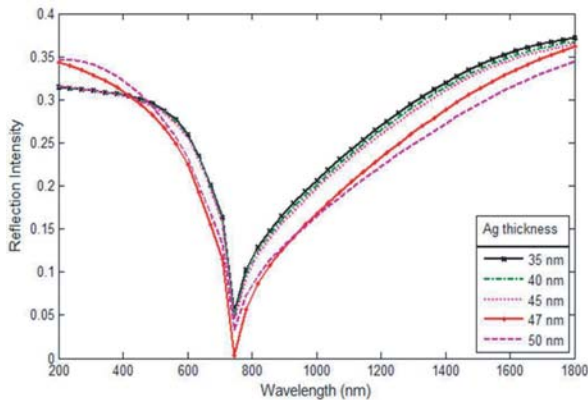
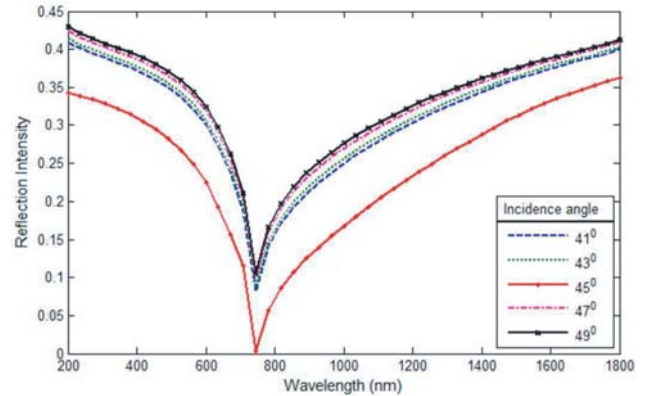
We investigated the influence of metallic layer thickness on the SPR sensor to get the optimized transfer of energy from the illuminating beam to the plasmon wave. Keeping the gold layer thickness constant at 2 nm and varying the silver layer thickness from 15 nm to 47 nm, the reflectivity was studied at the operating wavelength of 750 nm and is shown in Fig. 3. The lowest reflectivity dip was found with the Ag layer thickness of 47 nm. To find whether this thickness is related to the operating wavelength,

Table 1. Refractive indices of Ag, Au and Ti at 750 nm and 770 nm wavelengths (λ) [12, 25, 26].

Metal	λ (nm)	Real part	Imaginary part
Ag	750	0.1468	4.8604
	770	0.032151	5.3463
Au	750	0.1676	4.5332
	770	0.14430	4.6583
Ti	750	2.9838	4.0042
	770	3.0452	4.0100

in Fig. 4 we studied the spectral effects of different Ag film thicknesses on reflectance at an incidence angle of 45.34° . For Ag layer thickness of 47 nm, the lowest reflectivity is observed again at 750 nm, and the wavelength at which the lowest reflectivity is observed hardly changes with the thickness. It is important to examine the effects of incidence angle on wavelength-dependent SPR signals. Fig. 5 shows spectral effects of incidence angle from 41° to 49° on reflectance for the case of 47 nm Ag layer thickness and 2 nm Au layer thickness. Again at 750 nm with 45.34° incidence angle, the reflectance was sharper than in other cases.

Benefits of the bimetallic configuration can be realized by examining the performances of three configurations: having only Au layer, having only Ag layer and having coupled Ag-Au layer. For all three cases sensitivity and other parameters were studied with different layer thicknesses at the operating wavelength of 750 nm, and the optimized thicknesses were observed. Fig. 6(a) shows variation of sensitivity (SF) as a function of Au layer thickness with corresponding FWHM when only Au layer is used. A thickness of 2 nm provides the highest sensitivity ($62.65^\circ/\text{RIU}$), and FWHM (1.08648°) is mostly unaffected by Au layer thickness. CSF and other parameters for different Au layer thicknesses are summarized in Table 2(a). For Ag-only layer configuration, variations of sensitivity as well as FWHM with Ag layer thickness are shown in Fig. 6(b). In this case, 47 nm thickness of Ag layer provides the highest sensitivity ($70.65^\circ/\text{RIU}$) with the corresponding FWHM value of 0.193072° . If the Ag layer thickness is increased from 20 nm to 47 nm, FWHM is reduced significantly, but above 47 nm, there is almost no change of FWHM values. Table 2(b) summarizes other performance parameters. For coupled Ag-Au layer configuration, Fig. 6(c) shows the sensitivity and FWHM performances. (47 nm + 2 nm =) 49 nm thickness of Ag-Au couple layer gave the best sensitivity ($70.90^\circ/\text{RIU}$) and FWHM (0.189534°). For other thicknesses, different sensor performance parameters are given in Table 2(c). From Fig. 6(c) and Table 2(c) we see that for (50 nm + 3 nm =) 53 nm thickness of Ag-Au layer

**Figure 4.** Spectral effects of different Ag layer thicknesses on reflectance for a constant Au layer thickness of 2 nm and at 45.34° incidence angle.**Figure 5.** Spectral effects of incidence angle on reflectance for a constant Ag layer thickness of 47 nm and Au layer thickness of 2 nm.

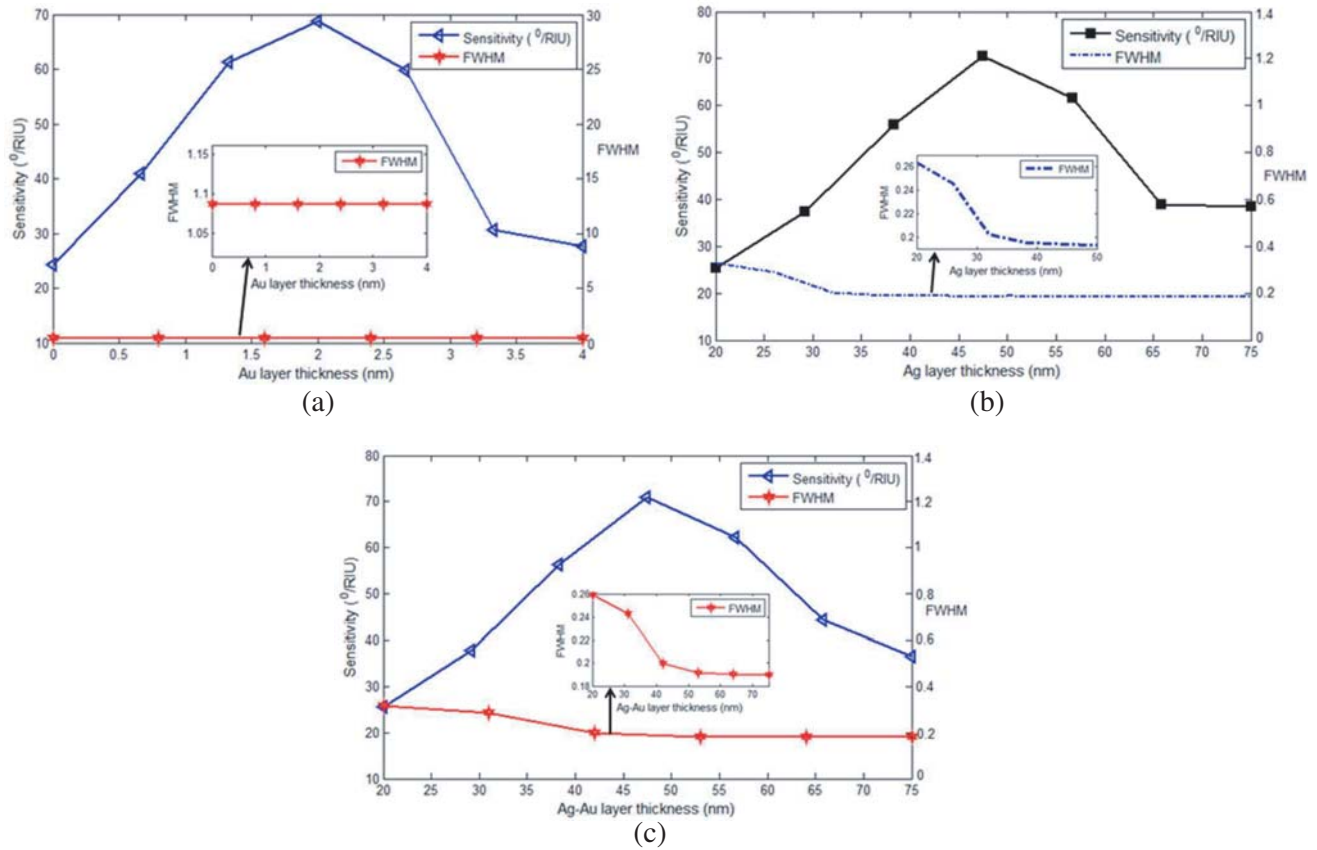


Figure 6. Variation of sensitivity and FWHM (a) as a function of Au layer thickness in Au-only configuration, (b) as a function of Ag layer thickness in Ag-only configuration and (c) as a function of couple Ag-Au layer thickness in couple Ag-Au layer configuration.

value of FWHM is better than that for (47 nm + 2 nm =)49 nm. However, when all performance issues, such as SF and reflectance at resonance, are taken into consideration, the overall figure of merit is given by CSF, and the best CSF is found with (47 nm + 2 nm =)49 nm thickness. From Figs. 6(a), 6(b) and Tables 2(a), 2(b) it is observed that for the single metal layer case, as expected, the sensor performance is better for only Ag layer than that for only Au layer. However, the coupled Ag-Au layer provides an overall better performance than the single metal layer configuration, and the optimized thicknesses are 47 nm for Ag and 2 nm for Au. The reflectivity curves with optimized metal layer thicknesses for the three configurations — only Au layer, only Ag layer and coupled Ag-Au layer — are shown in Fig. 7. The lowest and sharpest dip in the reflectivity curve is observed for coupled Ag-Au layer configuration.

As shown in Fig. 1, the proposed SPR sensor has an air gap layer. Table 3 shows that inclusion of this air gap layer enhances both the sensitivity (70.90°/RIU) and the CSF (372.8 RIU⁻¹) compared to the case where no such air gap is used (sensitivity of 66.29°/RIU and CSF of 285.0 RIU⁻¹). References [27, 28] also used an air gap layer which works as a dielectric medium and increases the resonance dip of the reflectivity curve. Table 3 also shows performances of the proposed sensor compared to the SPR sensor of [27] — both for the cases when air gap layer is present, and no air gap layer is there. The proposed SPR sensor has excellent CSF of 372.8 RIU⁻¹ in comparison with that of [27] which has the CSF of 200.0 RIU⁻¹. Sensitivity of the proposed sensor is also higher 70.90°/RIU against 66.79°/RIU. Compared to [27], better performance was observed for both cases of with and without air gap layer. Table 4 shows the optimized air gap layer thickness which is 15 nm.

Since both silver and gold have poor adherence to glass in the proposed SPR biosensor, a Ti layer is used for adherence of silver layer on prism glass. Also to further enhance the performance and for the purpose of protection, a thin InP layer is used between the metallic layer and the cover material

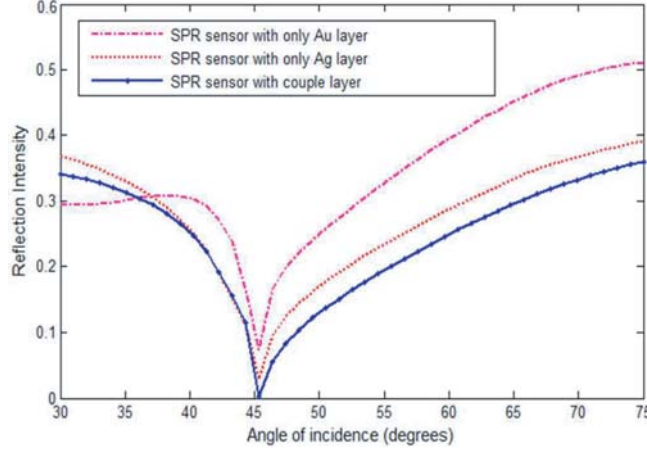


Figure 7. Reflectivity curves with optimized metal thicknesses for the three configurations-only Au layer, only Ag layer, and couple Ag-Au layer.

to be sensed. This layer enables surface plasmon to spread along it and causes a larger fraction of the evanescent field to be in the analyte region. The large refractive index of this layer causes the guidance of the wave for smaller thicknesses and makes the interaction volume larger. All these improve the sensor performance. Table 5 shows the performance improvement with thin InP layer against the cases

Table 2. Comparison of sensor performance parameters (a) for only Au layer configuration with different Au layer thicknesses, (b) for only Ag layer configuration with different Ag layer thicknesses and (c) for couple Ag-Au layer with different Ag-Au layer thicknesses.

(a)						
Thickness (nm) of Au		θ_{res} (deg)	R_r	SF (deg/RIU)	SM (deg ⁻¹)	CSF (RIU ⁻¹)
1		45.34	0.098436	45.44	0.590	26.81
2		45.34	0.074085	62.65	0.852	53.38
3		45.34	0.114638	40.54	0.447	18.12
(b)						
Thickness (nm) of Ag		θ_{res} (deg)	R_r	SF (deg/RIU)	SM (deg ⁻¹)	CSF (RIU ⁻¹)
45		45.34	0.0507289	66.72	4.301	287.0
47		45.34	0.0287826	70.65	5.030	355.4
50		45.34	0.0407289	68.54	4.732	324.3
(c)						
Thickness (nm)		θ_{res} (deg)	R_r	SF (deg/RIU)	SM (deg ⁻¹)	CSF (RIU ⁻¹)
Ag	Au					
45	1	45.34	0.0133912	69.89	4.624	323.2
47	2	45.34	0.00339201	70.90	5.258	372.8
50	3	45.34	0.0092168	70.37	4.981	350.5
1	45	45.34	0.0230499	69.85	4.077	284.8
2	47	45.34	0.0412693	67.98	3.382	230.0
3	50	45.34	0.0724667	67.57	3.208	216.8

Table 3. Comparative sensor performances of the proposed SPR sensor against that of [27] with and without air gap layer.

Configuration		θ_{res} (deg)	SF (deg/RIU)	SM (deg ⁻¹)	CSF (RIU ⁻¹)
Proposed SPR sensor	With air gap	45.34	70.90	5.258	372.8
	Without air gap	45.34	66.29	4.300	285.0
Reference [27]	With air gap	57.76	66.79	2.9942	200.0
	Without air gap	56.49	55.57	3.3753	187.6

Table 4. Optimization of air gap layer thickness.

Air gap thickness (nm)	θ_{res} (deg)	R_r	SF (deg/RIU)	SM (deg ⁻¹)	CSF (RIU ⁻¹)
10	45.34	0.0942092	68.86	2.861	197.0
15	45.34	0.00339201	70.90	5.258	372.8
20	45.34	0.113534	67.34	2.575	173.4

Table 5. Performance of the SPR sensor for different dielectric layer materials and without any dielectric layer.

Sensor design	θ_{res} (deg)	R_r	SF (deg/RIU)	SM (deg ⁻¹)	CSF (RIU ⁻¹)
With InP	45.34	0.00339201	70.90	5.258	372.8
With SiO ₂	45.34	0.140825	68.78	2.936	201.9
Without dielectrics	45.34	0.155412	65.66	2.719	178.5

Table 6. Performance comparison of the proposed bimetallic SPR sensor and the bimetallic SPR sensor of [14].

Configuration	θ_{res} (deg)	R_r	SF (deg/RIU)	SM (deg ⁻¹)	CSF (RIU ⁻¹)
Proposed SPR sensor	45.34	0.00339201	70.90	5.258	372.8
Reference [14]	50.45	0.235591	49.17	2.197	108.0

when no such layer is used and when SiO₂, which has a relatively lower refractive index, is used. Both sensitivity and CSF increase significantly, and InP performs better than SiO₂. An optimized InP layer thickness of 20 nm gave the best performance. The bimetallic SPR sensor proposed here is compared against the bimetallic SPR sensor of [14], and their overall performance parameters are shown in Table 6. Sensitivity factor of the proposed SPR sensor is far better than the sensor of [14] (70.90°/RIU against 49.17°/RIU) while CSF of the proposed sensor is more than three times higher (372.8 RIU⁻¹ against 108.0 RIU⁻¹).

For sensitivity and CSF measurements of the proposed SPR biosensor, we considered water ($n = 1.33$) as the reference sensing medium. In the biosensors, analyte present in the liquid sample is captured by biomolecular interaction and produces a local increase in the refractive index at the covering or sensing medium. To measure the proposed SPR biosensor's ability to detect small variations in concentration at the ng/mL level [29] the refractive index of the sensing medium (target material for

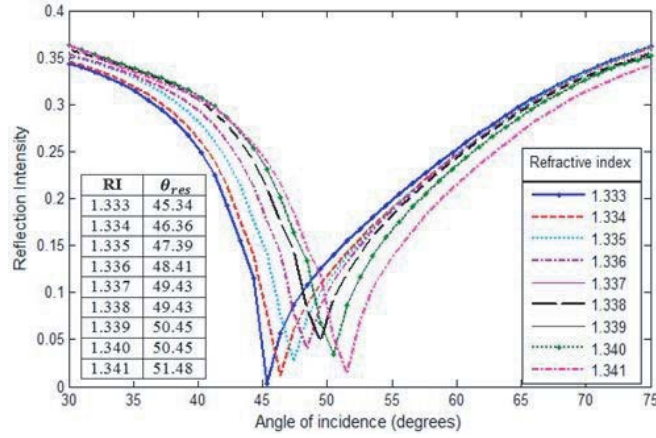


Figure 8. Changes of resonance angle (θ_{res}) for very small variation of refractive index (RI) of the sensing medium representing variations in analyte concentration.

sensing application) was varied from 1.333 to 1.341 with a step of 0.001. Variation of refractive index from 1.333 to 1.341 with a step of 0.001 covers the range of the solution with deoxygenated hemoglobin (HB) in phosphate-buffered saline solution up to 60% concentration (g/L) as reported in [30]. Fig. 8 shows that changes of concentration cause very minor changes in the refractive index (from 1.333 to 1.341) of the cover medium, and the dip of reflectance of the sensor is distinguishably shifted that means that the resonance angles are shifted with changed refractive indices. This demonstrates the proposed SPR sensor's ability to detect the variation of 1/1000 of RIU of the sensing medium (caused by concentration change of the analyte).

4. CONCLUSION

Design of a new bimetallic SPR sensor has been proposed. In addition to coupling Ag-Au films the proposed sensor has a thin InP layer on the metallic layer and also incorporates an air gap layer. We have shown that all these contribute to the overall performance improvement of the bimetallic SPR sensor. We established the best optical properties of the metals to obtain the best performance and optimized the thickness of each layer. Compared to the bimetallic SPR sensors that have been recently reported in the literature, sensitivity and overall figure of merit of the proposed sensor are far better. The proposed biosensor's capability to detect the variation of 1/1000 of RIU of the sensing medium (caused by concentration change of the analyte) has been demonstrated.

ACKNOWLEDGMENT

This work was supported by a research grant provided by University of Chittagong (Memo. No. 161/P&D/7-37(17)/2018).

REFERENCES

1. Nylander, C., B. Liedberg, and T. Lind, "Gas detection by means of surface plasmons resonance," *Sensors and Actuators*, Vol. 3, 79–88, 1982.
2. Liedberg, B., C. Nylander, and I. Lundström, "Surface plasmons resonance for gas detection and biosensing," *Sensors and Actuators*, Vol. 4, 299–304, 1983.
3. Viti, L., J. Hu, D. Coquillat, A. Politano, W. Knap, and M. S. Vitiello, "Efficient terahertz detection in black-phosphorus nano-transistors with selective and controllable plasma-wave, bolometric and thermoelectric response," *Scientific Reports*, Vol. 6, 20474, 2016.

4. Viti, L., D. Coquillat, A. Politano, K. A. Kokh, Z. S. Aliev, M. B. Babanly, O. E. Tereshchenko, W. Knap, E. V. Chulkov, and M. S. Vitiello, "Plasma-wave terahertz detection mediated by topological insulators surface states," *Nano Letters*, Vol. 16, No. 1, 80–87, 2016.
5. Shalabney, A. and I. Abdulhalim, "Sensitivity-enhancement methods for surface plasmon sensors," *Laser & Photonic Reviews*, Vol. 5, No. 4, 571–606, 2011.
6. Viti, L., A. Politano, and M. S. Vitiello, "Black phosphorus nanodevices at terahertz frequencies: Photodetectors and future challenges," *APL Materials*, Vol. 5, No. 3, 2017.
7. Agarwal, A., M. S. Vitiello, L. Viti, A. Cupolillo, and A. Politano, "Plasmonics with two-dimensional semiconductors: From basic research to technological applications," *Nanoscale*, Vol. 10, 8938–8946, 2018.
8. Politano, A., L. Viti, and M. Vitiello, "Optoelectronic devices, plasmonics, and photonics with topological insulators," *APL Materials*, Vol. 5, No. 3, 2017.
9. Politano, A., A. Cupolillo, G. D. Profio, H. Arafat, G. Chiarello, and E. Curcio, "When plasmonics meets membrane technology," *Journal of Physics Condensed Matter*, Vol. 28, No. 36, 2016.
10. Szunerits, S., N. Maalouli, E. Wijaya, J. Vilcot, and R. Boukherroub, "Recent advances in the development of graphene-based surface plasmon resonance (SPR) interfaces," *Analytical and Bioanalytical Chemistry*, Vol. 405, No. 5, 1435–1443, 2013.
11. Lecaruyer, P., M. Canva, and J. Rolland, "Metallic film optimization in a surface plasmon resonance biosensor by the extended Rouard method," *Applied Optics*, Vol. 46, No. 12, 2361, 2007.
12. Politano, A. and G. Chiarello, "The influence of electron confinement, quantum size effects, and film morphology on the dispersion and the damping of plasmonic modes in Ag and Au thin films," *Progress in Surface Science*, Vol. 90, No. 2, 144–193, 2015.
13. Politano, A., "Low-energy collective electronic mode at a noble metal interface," *Plasmonics*, Vol. 8, No. 2, 357–360, 2013.
14. Politano, A., V. Formoso, and G. Chiarello, "Dispersion and damping of gold surface plasmon," *Plasmonics*, Vol. 3, No. 4, 165–170, 2008.
15. Homola, J., "On the sensitivity of surface plasmon resonance sensors with spectral interrogation," *Sensors and Actuators B: Chemical*, Vol. 41, Nos. 1–3, 207–211, 1997.
16. Yuan, X., B. Ong, Y. Tan, D. Zhang, R. Irawan, and S. Tjin, "Sensitivity-stability-optimized surface plasmon resonance sensing with double metal layers," *Journal of Optics A: Pure and Applied Optics*, Vol. 8, No. 11, 959–963, 2006.
17. Ghorbanpour, M., "Optimization of sensitivity and stability of gold/silver bi-layer thin films used in surface plasmon resonance chips," *Journal of Nanostructures*, Vol. 3, 309–313, 2013.
18. Chen, Y., R. S. Zheng, D. G. Zhang, Y. H. Lu, P. Wang, H. Ming, Z. F. Luo, and Q. Kan, "Bimetallic chips for a surface plasmon resonance instrument," *Applied Optics*, Vol. 50, No. 3, 387–391, 2011.
19. Tran, N. H. T., B. T. Phan, W. J. Yoon, S. Khym, and H. Ju, "Dielectric metal-based multilayers for surface plasmon resonance with enhanced quality factor of the plasmonic waves," *Journal of Electronic Materials*, Vol. 46, No. 6, 3654–3659, 2017.
20. Chien, F.-C. and S.-J. Chen, "A sensitivity comparison of optical biosensors based on four different surface plasmon resonance modes," *Biosensors and Bioelectronics*, Vol. 20, No. 3, 633–642, 2004.
21. Aspnes, D. E. and A. A. Studna, "Dielectric functions and optical parameters of Si, Ge, GaP, GaAs, GaSb, InP, InAs, and InSb from 1.5 to 6.0 eV," *Physical Review B*, Vol. 27, 985–1009, 1983.
22. Lahav, A., M. Auslender, and I. Abdulhalim, "Sensitivity enhancement of guided-wave surface-plasmon resonance sensors," *Optics Letters*, Vol. 33, No. 21, 2539–2541, 2008.
23. Vlček, J., J. Pištora, and M. Lesňák, "Sensitivity enhancement in surface plasmon resonance sensors — Theoretical modeling," *Proceedings SPIE*, Vol. 7356, 735622, 2009.
24. Ong, B. H., X. Yuan, S. C. Tjin, J. Zhang, and H. M. Ng, "Optimized film thickness for maximum evanescent field enhancement of a bimetallic film surface plasmon resonance biosensor," *Sensors and Actuators B: Chemical*, Vol. 114, No. 2, 1028–1034, 2006.

25. Johnson, P. B. and R. W. Christy, "Optical constants of the noble metals," *Physical Review B*, Vol. 6, 4370–4379, 1972.
26. Johnson, P. B. and R. W. Christy, "Optical constants of transition metals: Ti, V, Cr, Mn, Fe, Co, Ni, and Pd," *Physical Review B*, Vol. 9, 5056–5070, 1974.
27. Verma, A., A. Prakash, and R. Tripathi, "Sensitivity enhancement of surface plasmon resonance biosensor using graphene and air gap," *Optics Communications*, Vol. 357, 106–112, 2015.
28. Yu, Z. and S. Fan, "Extraordinarily high spectral sensitivity in refractive index sensors using multiple optical modes," *Optics Express*, Vol. 19, No. 11, 10029–10040, 2011.
29. Zeng, S., K. V. Sreekanth, J. Shang, T. Yu, C.-K. Chen, F. Yin, D. Baillargeat, P. Coquet, H.-P. Ho, A. V. Kabashin, and K.-T. Yong, "Graphene-gold metasurface architectures for ultra sensitive plasmonic biosensing," *Advanced Materials*, Vol. 27, No. 40, 6163–6169, 2015.
30. Zhernovaya, O., O. Sydoruk, V. Tuchin, and A. Douplik, "The refractive index of human hemoglobin in the visible range," *Physics in Medicine and Biology*, Vol. 56, No. 13, 4013–4021, 2011.